

LETTER TO THE EDITOR

# The complexity of Orion: an ALMA view<sup>★</sup>

## II. gGg'-Ethylene Glycol and Acetic Acid

C. Favre<sup>1</sup>, L. Pagani<sup>2</sup>, P. Goldsmith<sup>3</sup>, E. Bergin<sup>4</sup>, M. Carvajal<sup>5,6</sup>, I. Kleiner<sup>7</sup>, G. Melnick<sup>8</sup>, and R. Snell<sup>9</sup>

<sup>1</sup> INAF-Osservatorio Astrofisico di Arcetri, Largo E. Fermi 5, Firenze, 50125, Italy  
e-mail: cfavre@arcetri.astro.it

<sup>2</sup> LERMA, UMR 8112 du CNRS, Observatoire de Paris, 61 Av. de l'Observatoire, 75014 Paris, France

<sup>3</sup> Jet Propulsion Laboratory, California Institute of Technology, 4800 Oak Grove Drive, Pasadena, CA 91109, USA

<sup>4</sup> Department of Astronomy, University of Michigan, 500 Church Street, Ann Arbor, MI 48109, USA

<sup>5</sup> Dpto. Ciencias Integradas, Unidad GIFMAN-UHU Asociada al CSIC, Universidad de Huelva, 21071, Huelva, Spain

<sup>6</sup> Instituto Universitario Carlos I de Física Teórica y Computacional, Universidad de Granada, Granada, Spain

<sup>7</sup> Laboratoire Interuniversitaire des Systèmes Atmosphériques (LISA), CNRS, UMR 7583, Université de Paris-Est et Paris Diderot, 61, Av. du Général de Gaulle, F-94010 Créteil Cedex, France

<sup>8</sup> Harvard-Smithsonian Center for Astrophysics, Cambridge, Massachusetts, USA

<sup>9</sup> Department of Astronomy, University of Massachusetts, Amherst, MA, 01003, USA

Received September 15, 1996; accepted March 16, 1997

### ABSTRACT

We report the first detection and high angular resolution ( $1.8'' \times 1.1''$ ) imaging of acetic acid ( $\text{CH}_3\text{COOH}$ ) and gGg'-ethylene glycol (gGg'( $\text{CH}_2\text{OH}$ )<sub>2</sub>) towards the Orion Kleinmann-Low nebula. The observations were carried out at  $\sim 1.3\text{mm}$  with ALMA during the Cycle 2. A notable result is that the spatial distribution of the acetic acid and ethylene glycol emission differs from that of the other O-bearing molecules within Orion-KL. Indeed, while the typical emission of O-bearing species harbors a morphology associated with a "V-shape" linking the Hot Core region to the Compact Ridge (with an extension towards the BN object), that of acetic acid and ethylene glycol mainly peaks at about  $2''$  southwest from the hot core region (near sources I and n). We find that the measured  $\text{CH}_3\text{COOH}:\text{aGg}'(\text{CH}_2\text{OH})_2$  and  $\text{CH}_3\text{COOH}:\text{gGg}'(\text{CH}_2\text{OH})_2$  ratios differ from the ones measured towards the low-mass protostar IRAS 16293-2422 by more than one order of magnitude. Our best hypothesis to explain these findings is that  $\text{CH}_3\text{COOH}$ , aGg'( $\text{CH}_2\text{OH}$ )<sub>2</sub> and gGg'( $\text{CH}_2\text{OH}$ )<sub>2</sub> are formed on the icy-surface of grains and then released into the gas-phase, via co-desorption with water, due to a bullet of matter ejected during the explosive event that occurred in the heart of the Nebula about 500-700 years ago.

**Key words.** Astrochemistry – ISM: molecules – Radio lines: ISM

### 1. Introduction

The Orion Kleinmann-Low nebula (hereafter Orion-KL) is the closest high mass-star forming region ( $388 \pm 5$  pc, Kounkel et al. 2017). Its proximity and rich molecular composition make this region well-suited for astrochemical study. In this context, numerous single-dish surveys, including the broadband Herschel/HIFI HEXOS survey (Bergin et al. 2010; Crockett et al. 2014), as well as interferometric observations have been performed towards this region (e.g. Favre et al. 2015; Pagani et al. 2017, and references therein). It is important to note that two main molecular components are associated with Orion-KL: the Compact Ridge and the Hot Core. The latter region may have resulted from interaction of the surrounding gas with remnants of the explosive event – triggered by the close encounter of the sources I, n and the BN object – that occurred in the region about 500–700 years ago (e.g. see, Zapata et al. 2011; Nissen et al.

2012, and references therein). Thus, the complex physical structure and history make Orion-KL an interesting source – that may not be representative of other high-mass star forming regions – to study the production route (at the icy surface of grains and/or in the gas phase) of complex organic molecules (i.e. molecules that contain six or more atoms, including carbon, hereafter COMs, see Herbst & van Dishoeck 2009). Although present in other star-forming regions, some COMs have not yet been detected in Orion-KL. This mainly results from sensitivity limitation and a high spectral confusion level (e.g. see, Tercero et al. 2010). High resolution and sensitivity, as offered by ALMA, are thus mandatory to search for weak lines associated with COMs. In that context, we have used ALMA during Cycle 2 to perform deep observations of this region in a fraction of band 6 ( $\approx 1-2$  mm).

Our ALMA-Cycle 2 data and first results are given in a companion paper by Pagani et al. (2017, hereafter Paper I). In this Letter, we focus on acetic acid ( $\text{CH}_3\text{COOH}$ ) and the gGg' conformer of ethylene glycol (gGg'( $\text{CH}_2\text{OH}$ )<sub>2</sub>) and report their first detection in Orion-KL. The detection of acetic acid in Orion-KL has not yet been reported, although a few transitions may be present in the IRAM 30m survey by Tercero et al. (2011). How-

<sup>★</sup> This paper makes use of the following ALMA data: ADS/JAO.ALMA#2013.1.00533.S. ALMA is a partnership of ESO (representing its member states), NSF (USA) and NINS (Japan), together with NRC (Canada), NSC and ASIAA (Taiwan), and KASI (Republic of Korea), in cooperation with the Republic of Chile. The Joint ALMA Observatory is operated by ESO, AUI/NRAO and NAOJ.

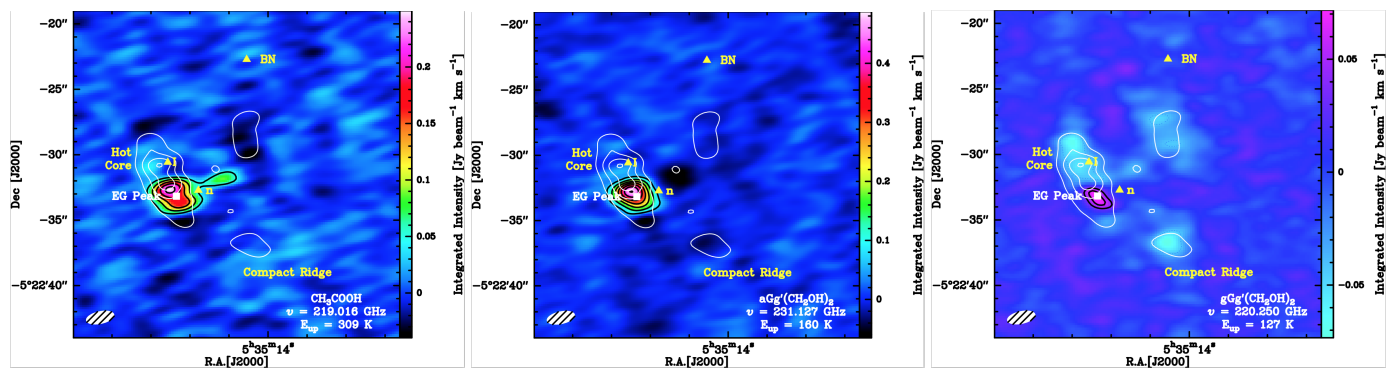


**Fig. 1.** *Left Panel:*  $\text{CH}_3\text{COOH}$  integrated emission map at 219016 MHz. The first contour and the level step are at  $5\sigma$  (where  $1\sigma=9.3\times 10^{-3}$  Jy beam $^{-1}$  km s $^{-1}$ ). *Middle Panel:*  $\text{aGg}'(\text{CH}_2\text{OH})_2$  integrated emission map at 231127 MHz. The first contour and the level step are at  $5\sigma$  (where  $1\sigma=1.4\times 10^{-2}$  Jy beam $^{-1}$  km s $^{-1}$ ). *Right Panel:*  $\text{gGg}'(\text{CH}_2\text{OH})_2$  integrated emission map at 220250 MHz. The contour levels are at  $-4$ ,  $4$  and  $6\sigma$  (where  $1\sigma=1\times 10^{-2}$  Jy beam $^{-1}$  km s $^{-1}$ ). A narrow  $v_{\text{LSR}}$  interval (from 7 to 9 km/s) has been selected to reduce confusion by nearby lines (see Section 3.3 and Appendix C). Positions of the radio source I, the BN object and the IR source n (see Goddi et al. 2011) are indicated by yellow triangles. The white square indicates the position of the Ethylene Glycol Peak ( $\alpha_{J2000} = 05^{\text{h}}35^{\text{m}}14^{\text{s}}.47$ ,  $\delta_{J2000} = -05^{\circ}22'33''.17$ ) by BD15. Finally, the continuum emission at 235 GHz is overlaid in white contours with a level step of  $0.2$  Jy beam $^{-1}$  (Paper I).

ever, this species is known to be present in low-mass and high-mass star forming regions (e.g. Remijan et al. 2003; Shiao et al. 2010; Jørgensen et al. 2016). Regarding  $\text{gGg}'$ -Ethylene glycol, this conformer has only been detected toward the Class 0 protostar IRAS 16293–2422 by Jørgensen et al. (2016). Incidentally, the most stable conformer of ethylene glycol ( $\text{aGg}'$ ) is detected towards low-mass, intermediate-mass and high-mass sources, including Orion-KL (see e.g. Fuente et al. 2014; Lykke et al. 2015; Brouillet et al. 2015; Rivilla et al. 2017, and references therein). In Section 2 we briefly describe our ALMA observations. Results and analysis are given and discussed in Sections 3 and 4, respectively.

## 2. Observations and data reduction

Acetic acid and ethylene glycol lines towards Orion-KL were observed with 37 antennas on 2014 December 29 and 39 antennas on 2014 December 30. The two following phase-tracking centers were used to perform the observations:  $\alpha_{J2000} = 05^{\text{h}}35^{\text{m}}14^{\text{s}}.16$ ,  $\delta_{J2000} = -05^{\circ}22'31''.504$  and  $\alpha_{J2000} = 05^{\text{h}}35^{\text{m}}13^{\text{s}}.477$ ,  $\delta_{J2000} = -05^{\circ}22'08''.50$ . The observations lie in the frequency range 215.15 GHz to 252.04 GHz in band 6 and cover about 16 GHz of effective bandwidth with spectral resolution of about  $0.7$  km s $^{-1}$ . Data reduction and continuum subtraction were performed through the Common Astronomy Software Applications (CASA) software (McMullin et al. 2007). The cleaning of the spectral lines was performed using the GILDAS software<sup>1</sup>. The resulting synthesized beam is typically  $1.8'' \times 1.1''$  (P.A. of  $84^{\circ}$ ). For further details, see Paper I.

## 3. Data analysis and results

### 3.1. Acetic acid and Ethylene glycol molecular frequencies

We used the spectroscopic data parameters from Ilyushin et al. (2008) and Ilyushin et al. (2013) for acetic acid, with the following line selection criteria: Einstein spontaneous emission coefficient  $A_{ij} \geq 5\times 10^{-5}$  s $^{-1}$  and upper level energy  $E_{\text{up}} \leq 400$  K. For the partition function we adopt the complete rotational-torsional-vibrational partition function given by Calcutt, Woods, Carvajal et al. (to be submitted to MNRAS).

<sup>1</sup> <http://www.iram.fr/IRAMFR/GILDAS/>

For both ethylene glycol conformers we used the spectroscopic data parameters from Christen & Müller (2003) and Müller & Christen (2004) that are available from the Cologne Database for Molecular Spectroscopy catalog (CDMS, Müller et al. 2005). More specifically, we searched for transitions up to  $E_{\text{up}} \approx 400$  K, and  $A_{ij} \geq 1\times 10^{-4}$  s $^{-1}$ . The energy difference between the two conformers is about  $200$  cm $^{-1}$ , the more stable conformer being the  $\text{aGg}'$ -ethylene Glycol (Müller & Christen 2004). Further details about the difference between the  $\text{aGg}'$  and the  $\text{gGg}'$  conformer can be found in Brouillet et al. (2015, hereafter BD15).

### 3.2. LTE Modeling

Our analysis is based on the assumption that local thermodynamic equilibrium (LTE) is reached. This assumption is reasonable given that LTE modeling of a thousand emissive transitions assigned to simple and complex molecules fits well the HIFI/Herschel observations performed towards Orion-KL (see Crockett et al. 2014). In addition, we assume that all the species emit at the same rotational temperature within the same source size. We use the CLASS extension WEEDS (Maret et al. 2011) to model the acetic acid and ethylene glycol (both  $\text{aGg}'$  and  $\text{gGg}'$  conformer) emission, that we assume to be optically thin. We used the values derived for  $\text{aGg}'(\text{CH}_2\text{OH})_2$  by BD15 as input parameter to initialize our models.

### 3.3. Emission map

The  $\text{CH}_3\text{COOH}$ ,  $\text{aGg}'(\text{CH}_2\text{OH})_2$  and  $\text{gGg}'(\text{CH}_2\text{OH})_2$  emission maps integrated over the line profile are shown in Figure 1. The nominal velocity of Orion-KL is  $v_{\text{LSR}}=7.6$  km s $^{-1}$ . It is important to note that the northwest extension seen in the acetic acid emission map is due to contamination by a U-line (see Appendix C) and is not related to the acetic acid emission. Indeed, although we use a restricted  $v_{\text{LSR}}$  interval to produce the maps, confusion still dominates the region (Paper I).

A salient result is that the distribution of the emission associated with these molecules is similar within the beam and the main emission peak is located about  $2''$  southwest of the hot core, near both radio source I and IR source n. This peak corresponds to the "Ethylene Glycol Peak" (hereafter EGP) identi-

**Table 1.** Best fit line parameters and derived peak column densities for acetic acid and ethylene glycol towards Orion–KL EGP.

Molecule	Component 1				Component 2			
	$v$ (km s <sup>-1</sup> )	$\Delta v_{1/2}$ (km s <sup>-1</sup> )	$T_{\text{rot}}$ (K)	$N$ (10 <sup>15</sup> cm <sup>-2</sup> )	$v$ (km s <sup>-1</sup> )	$\Delta v_{1/2}$ (km s <sup>-1</sup> )	$T_{\text{rot}}$ (K)	$N$ (10 <sup>15</sup> cm <sup>-2</sup> )
CH <sub>3</sub> COOH	7.9	2.5	140	12	5.1	2.3	140	3.3
aGg'(CH <sub>2</sub> OH) <sub>2</sub>	7.8	2.1	140	6.8	5.1	2.1	140	1.5
gGg'(CH <sub>2</sub> OH) <sub>2</sub>	7.8	2.1	140	2.7	5.1	2.1	140	0.66

fied by BD15 for the aGg'(CH<sub>2</sub>OH)<sub>2</sub> conformer. An outstanding result is that, as for the aGg'(CH<sub>2</sub>OH)<sub>2</sub> molecule (BD15), the distribution of the emission associated with the acetic acid and the gGg'-ethylene glycol conformer differs from that of typical O-bearing species within Orion-KL. Indeed, the emission of the targeted species appears to come from a compact source in the vicinity of the Hot Core region while the emission associated with O-bearing molecules, such as methyl formate (e.g. see Favre et al. 2011, and Appendix D), is generally described by an extended V-shape within Orion-KL linking the Hot Core component to the Compact Ridge region and extending towards the BN object (e.g., Guélin et al. 2008).

### 3.4. Spectra

Spectra of a sample of the most intense transitions (i.e. emitting above the 5 $\sigma$  level) of acetic acid (15 transitions from  $E_{\text{up}}=70$  K up to 318 K, including 5 unblended), aGg' ethylene glycol (50 transitions from  $E_{\text{up}}=111$  K up to 266 K, including 19 unblended) and gGg' ethylene glycol (22 transitions from  $E_{\text{up}}=102$  K up to 216 K, including 5 unblended) towards the EGP region are displayed in Figs 2, 3 and 4, respectively. In addition, our best "by eye" WEEDS fits together with the sum of the modeled emission from all the other species in the region (Paper I) are also overlaid in these figures. Tables B.1, B.2 and B.3 in Appendix B, list the spectroscopic line parameters for the displayed acetic acid, aGg'-ethylene glycol and gGg'-ethylene glycol transitions, respectively. The bulk of the emission associated with the targeted molecules peaks at about 7.8–7.9 km s<sup>-1</sup>. Nonetheless, all the line profiles display an extended blue-shifted wing. Thus, two velocity components, one around 8 km s<sup>-1</sup> and the other one at about 5 km s<sup>-1</sup>, are required to fit the emission. The model parameters that best reproduce the ALMA observations of acetic acid and ethylene glycol (both conformers) in the direction of the EGP region are summarized in Table 1. In the present analysis we assume an overall uncertainty in the range 30%–40%.

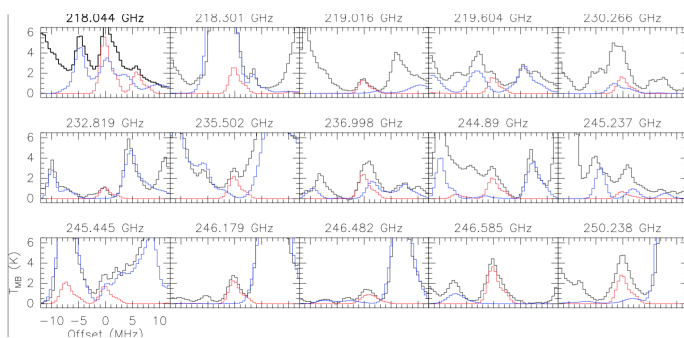


**Fig. 2.** ALMA observations (black) overlaid with the WEEDS model for acetic acid (red). The sum of the modeled emission from all the other species is overlaid in blue (Paper I).

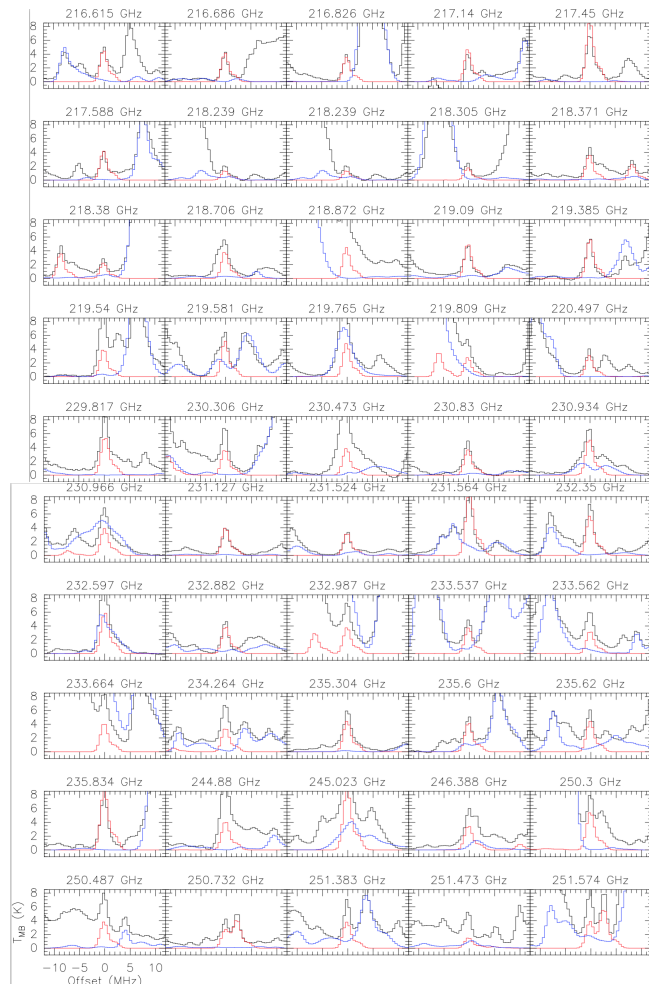


**Fig. 3.** ALMA observations (black) overlaid with the WEEDS model for aGg' ethylene glycol (red). The sum of the modeled emission from all the other species is overlaid in blue (Paper I).

### 3.5. Column densities and Relative abundances

Table 1 gives the derived CH<sub>3</sub>COOH, aGg'(CH<sub>2</sub>OH)<sub>2</sub> and gGg'(CH<sub>2</sub>OH)<sub>2</sub> peak column densities assuming a source size of 3'' for each velocity component. We note that our best aGg'(CH<sub>2</sub>OH)<sub>2</sub> fit result ( $v$ ,  $\Delta v$ ,  $T_{\text{rot}}$  and  $N$ ) is consistent within the uncertainties (~30%-40%) with the value reported by BD15.

Table 2 lists the relative abundance ratios for acetic acid and ethylene glycol derived from our best model results (see Table 1) towards both velocity components observed in direction of the EGP peak. The derived abundance ratios are equal within the error bars for both velocity components. It is important to note that BD15 reported an upper limit on the aGg'(CH<sub>2</sub>OH)<sub>2</sub>/gGg'(CH<sub>2</sub>OH)<sub>2</sub> ratio of 5. This discrepancy apparently results from an underestimate of the limit on the gGg'(CH<sub>2</sub>OH)<sub>2</sub> column density by BD15.

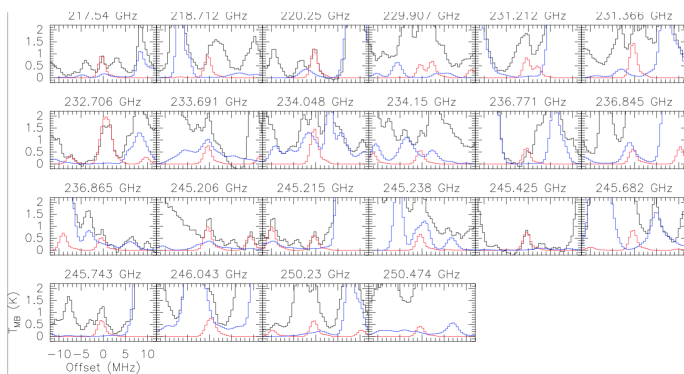


**Fig. 4.** ALMA observations (black) overlaid with the WEEDS model for gGg' ethylene glycol (red). The sum of the modeled emission from all the other species is overlaid in blue (Paper I).

**Table 2.** Relative abundances.

Component	$\frac{\text{CH}_3\text{COOH}}{\text{aGg}'(\text{CH}_2\text{OH})_2}$	$\frac{\text{CH}_3\text{COOH}}{\text{gGg}'(\text{CH}_2\text{OH})_2}$	$\frac{\text{aGg}'(\text{CH}_2\text{OH})_2}{\text{gGg}'(\text{CH}_2\text{OH})_2}$
8 km s <sup>-1</sup>	1.8	4.4	2.5
5 km s <sup>-1</sup>	2.4	5.0	2.3

**Notes.** The given values have uncertainties of 40%–50%.

## 4. Discussion

In Figure 5, we show the relative abundance ratios,  $\text{CH}_3\text{COOH}:\text{aGg}'(\text{CH}_2\text{OH})_2:\text{gGg}'(\text{CH}_2\text{OH})_2$ , derived in this study along with the ones derived towards the low-mass protostar IRAS 16293–2422 by Jørgensen et al. (2016). It is immediately apparent that the  $\text{CH}_3\text{COOH}:(\text{CH}_2\text{OH})_2$  ratios measured in direction of Orion-KL are larger than those of the low-mass protostar IRAS 16293–2422 by over an order of magnitude. Also, we note that the  $\text{aGg}'(\text{CH}_2\text{OH})_2:\text{gGg}'(\text{CH}_2\text{OH})_2$  ratio seems to be, within the error bars, the same for both regions. The fact that Jørgensen et al. (2016) assumed different rotational temperatures for the two conformers to estimate this ratio might explain the slight difference. Lykke et al. (2015) have shown that the source luminosities are likely correlated with relative abundances of complex organic molecules. These findings lead one to ask whether and how the physical conditions in these regions, in particular Orion-KL, impact the production and the possible release to the gas-phase, of these species.

Both  $\text{CH}_3\text{COOH}$  and  $(\text{CH}_2\text{OH})_2$  are believed to mainly be formed on the icy-surface of grains, although gas-phase formation routes cannot be ruled out (see e.g. Laas et al. 2011; Rivilla et al. 2017). Interestingly enough, Garrod et al. (2008) have shown that ethylene glycol is produced more efficiently in grain mantles in comparison to acetic acid by at least one order of magnitude. This naturally explains the observation that the abundance ratio  $\text{CH}_3\text{COOH}/(\text{CH}_2\text{OH})_2$  is lower in low-mass star forming regions. However, regarding Orion-KL, an additional mechanism is required to explain the over abundance of  $\text{CH}_3\text{COOH}$ . It is noteworthy that Wright & Plambeck (2017) have recently proposed that a bullet of matter ejected during the explosive event that occurred  $\sim 500$ –700 years ago (Nissen et al. 2012) has impacted the EGP region. More specifically, using high angular resolution ALMA observations, Wright & Plambeck (2017) have reported the presence of a molecular ring in  $\text{HC}_3\text{N}$ ,  $\text{HCN}$  and  $\text{SO}_2$  which is not associated with continuum emission. In that context, it is important to note that the distribution of the acetic acid and ethylene glycol is co-spatial with this

ring (Figure E.1 in Appendix E). In addition, both acetic acid and ethylene glycol line profiles present a blue-shifted emission wing (i.e. the 5 km s<sup>-1</sup> velocity component), this specific asymmetric line profile being also observed for other molecules in this region (e.g. methanol, formic acid, Paper I). These findings strongly suggest that this region is peculiar and is different from other star-forming regions. Indeed, the impact that took place here has led to the release of icy COMs in the gas-phase, generating the observed gas motions together with a rich molecular composition that may reflect gas-phase chemistry in an induced shock/post-shock stage.

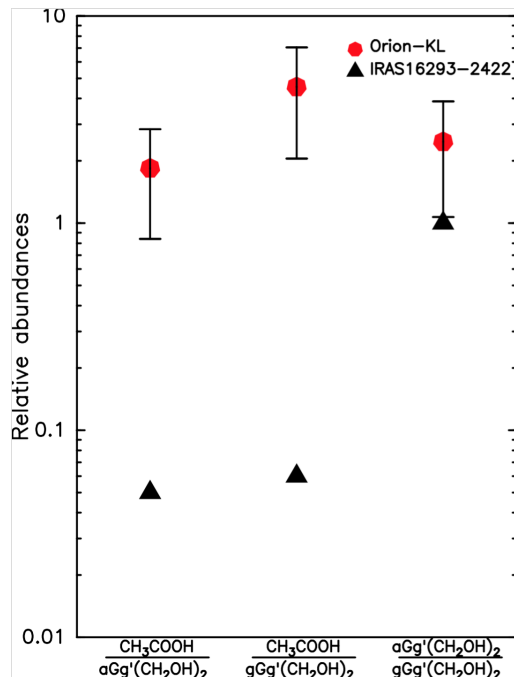


**Fig. 5.** Acetic acid and ethylene glycol abundance ratios towards Orion-KL (red circles, this study) and IRAS 16293-2422 (black triangles, Jørgensen et al. 2016). The ratios for Orion-KL are obtained from the sum of the velocity components given in Table 1.

*Acknowledgements.* See Appendix A.

## References

- Bergin, E. A., Phillips, T. G., Comito, C., et al. 2010, *A&A*, 521, L20  
Brouillet, N., Despois, D., Lu, X.-H., et al. 2015, *A&A*, 576, A129  
Christen, D. & Müller, H. S. P. 2003, *Physical Chemistry Chemical Physics (Incorporating Faraday Transactions)*, 5, 3600  
Crockett, N. R., Bergin, E. A., Neill, J. L., et al. 2014, *ApJ*, 787, 112  
Favre, C., Bergin, E. A., Neill, J. L., et al. 2015, *ApJ*, 808, 155  
Favre, C., Despois, D., Brouillet, N., et al. 2011, *A&A*, 532, A32  
Fuente, A., Cernicharo, J., Caselli, P., et al. 2014, *A&A*, 568, A65  
Garrod, R. T., Weaver, S. L. W., & Herbst, E. 2008, *ApJ*, 682, 283  
Goddi, C., Humphreys, E. M. L., Greenhill, L. J., Chandler, C. J., & Matthews, L. D. 2011, *ApJ*, 728, 15  
Guélin, M., Brouillet, N., Cernicharo, J., Combes, F., & Wooten, A. 2008, *Ap&SS*, 313, 45  
Herbst, E. & van Dishoeck, E. F. 2009, *ARA&A*, 47, 427  
Ilyushin, V., Kleiner, I., & Lovas, F. J. 2008, *Journal of Physical and Chemical Reference Data*, 37, 97  
Ilyushin, V. V., Endres, C. P., Lewen, F., Schlemmer, S., & Drouin, B. J. 2013, *Journal of Molecular Spectroscopy*, 290, 31  
Jørgensen, J. K., van der Wiel, M. H. D., Coutens, A., et al. 2016, *A&A*, 595, A117  
Kounkel, M., Hartmann, L., Loinard, L., et al. 2017, *ApJ*, 834, 142  
Laas, J. C., Garrod, R. T., Herbst, E., & Widicus Weaver, S. L. 2011, *ApJ*, 728, 71

- Lykke, J. M., Favre, C., Bergin, E. A., & Jørgensen, J. K. 2015, *A&A*, 582, A64
- Maret, S., Hily-Blant, P., Pety, J., Bardeau, S., & Reynier, E. 2011, *A&A*, 526, A47
- McMullin, J. P., Waters, B., Schiebel, D., Young, W., & Golap, K. 2007, in *Astronomical Society of the Pacific Conference Series*, Vol. 376, *Astronomical Data Analysis Software and Systems XVI*, ed. R. A. Shaw, F. Hill, & D. J. Bell, 127
- Müller, H. S. P. & Christen, D. 2004, *Journal of Molecular Spectroscopy*, 228, 298
- Müller, H. S. P., Schlöder, F., Stutzki, J., & Winnewisser, G. 2005, *Journal of Molecular Structure*, 742, 215
- Nissen, H. D., Cunningham, N. J., Gustafsson, M., et al. 2012, *A&A*, 540, A119
- Pagani, L., Favre, C., Goldsmith, P. F., et al. 2017, *A&A*, Paper I, in press
- Remijan, A., Snyder, L. E., Friedel, D. N., Liu, S., & Shah, R. Y. 2003, *ApJ*, 590, 314
- Rivilla, V. M., Beltrán, M. T., Cesaroni, R., et al. 2017, *A&A*, 598, A59
- Shiao, Y., Looney, L. W., Remijan, A. J., Snyder, L. E., & Friedel, D. N. 2010, *ApJ*, 716, 286
- Tercero, B., Cernicharo, J., Pardo, J. R., & Goicoechea, J. R. 2010, *A&A*, 517, A96
- Tercero, B., Vincent, L., Cernicharo, J., Viti, S., & Marcelino, N. 2011, *A&A*, 528, A26+
- Wright, M. C. H. & Plambeck, R. L. 2017, *ArXiv e-prints* [[arXiv:1705.03957](https://arxiv.org/abs/1705.03957)]
- Zapata, L. A., Schmid-Burgk, J., & Menten, K. M. 2011, *A&A*, 529, A24

## Appendix A: Acknowledgements

CF acknowledges support from the Italian Ministry of Education, Universities and Research, project SIR (RBSI14ZRHR). The authors thank Hannah Calcutt for providing the acetic acid partition function. We also thank Melvyn Wright and Rick Plambeck for their HC<sub>3</sub>N emission map. This work was carried out in part at the Jet Propulsion Laboratory, which is operated for NASA by the California Institute of Technology. MC acknowledges financial funding from the project FIS2014-53448-C2-2-P (MINECO, Spain), and CMST COST Action CM1405 MOLIM. CF and MC acknowledge support from CMST COST Action CM1401 Our Astro-Chemical History. LP thanks Arnaud Belloche and H.S.P. Müller for their help with molecular spectroscopy data. CF thanks Claudio Codella for enlightening discussion on shocks. Finally, CF thanks Vianney Taquet and Franck Hersant for fruitful discussion about the binding energies and acetic acid formation routes.

## Appendix B: Spectroscopic line parameters

Tables B.1, B.2 and B.3 list the spectroscopic line parameters for the acetic acid, aGg'-ethylene glycol and gGg'-ethylene glycol lines that are displayed in Figures 2, 3 and 4, respectively.



**Table B.1.** Spectroscopic data of the acetic acid lines displayed in Fig. 2

Frequency (MHz)	Symmetry	Quantum number		$A_{ul}$ ( $s^{-1}$ )	$g_{up}$	$E_{up}$ (K)
		$J_{K_a, K_c}, v_t$ (up)	$J_{K_a, K_c}, v_t$ (low)			
218044.2146	A	$20_{(0,20), v_t=0}$	$19_{(1,19), v_t=0}$	2.25e-05	82	112.2
218044.2146	A	$20_{(1,20), v_t=0}$	$19_{(0,19), v_t=0}$	2.25e-05	82	112.2
218044.2146	A	$20_{(0,20), v_t=0}$	$19_{(0,19), v_t=0}$	6.06e-05	82	112.2
218044.2146	A	$20_{(1,20), v_t=0}$	$19_{(1,19), v_t=0}$	6.06e-05	82	112.2
218301.0685	E	$20_{(0,20), v_t=1}$	$19_{(0,19), v_t=1}$	2.44e-08	82	217.4
218301.0685	E	$20_{(1,20), v_t=1}$	$19_{(1,19), v_t=1}$	2.44e-08	82	217.4
218301.0685	E	$20_{(0,20), v_t=1}$	$19_{(1,19), v_t=1}$	8.31e-05	82	217.4
218301.0685	E	$20_{(1,20), v_t=1}$	$19_{(0,19), v_t=1}$	8.31e-05	82	217.4
219016.0364	E	$20_{(0,20), v_t=2}$	$19_{(1,19), v_t=2}$	6.41e-05	82	309.0
219016.0365	E	$20_{(0,20), v_t=2}$	$19_{(0,19), v_t=2}$	1.77e-05	82	309.0
219016.0385	E	$20_{(1,20), v_t=2}$	$19_{(1,19), v_t=2}$	1.77e-05	82	309.0
219016.0386	E	$20_{(1,20), v_t=2}$	$19_{(0,19), v_t=2}$	6.41e-05	82	309.0
219603.9437	A	$20_{(0,20), v_t=2}$	$19_{(1,19), v_t=2}$	6.51e-06	82	289.1
219603.9437	A	$20_{(1,20), v_t=2}$	$19_{(1,19), v_t=2}$	7.77e-05	82	289.1
219603.9446	A	$20_{(1,20), v_t=2}$	$19_{(0,19), v_t=2}$	6.51e-06	82	289.1
219603.9446	A	$20_{(0,20), v_t=2}$	$19_{(0,19), v_t=2}$	7.77e-05	82	289.1
230266.0061	A	$21_{(0,21), v_t=2}$	$20_{(1,20), v_t=2}$	2.71e-05	86	300.2
230266.0061	A	$21_{(1,21), v_t=2}$	$20_{(0,20), v_t=2}$	2.71e-05	86	300.2
230266.0061	A	$21_{(0,21), v_t=2}$	$20_{(0,20), v_t=2}$	7.02e-05	86	300.2
230266.0061	A	$21_{(1,21), v_t=2}$	$20_{(1,20), v_t=2}$	7.02e-05	86	300.2
232818.7007	E	$19_{(2,17), v_t=2}$	$18_{(3,16), v_t=2}$	7.31e-05	78	317.7
232818.7077	E	$19_{(3,17), v_t=2}$	$18_{(3,16), v_t=2}$	1.06e-05	78	317.7
232818.7318	E	$19_{(2,17), v_t=2}$	$18_{(2,16), v_t=2}$	1.06e-05	78	317.7
232818.7388	E	$19_{(3,17), v_t=2}$	$18_{(2,16), v_t=2}$	7.31e-05	78	317.7
235501.6832	A	$20_{(2,18), v_t=1}$	$19_{(3,17), v_t=1}$	3.21e-05	82	241.5
235501.6832	A	$20_{(3,18), v_t=1}$	$19_{(2,17), v_t=1}$	3.21e-05	82	241.5
235501.6832	A	$20_{(2,18), v_t=1}$	$19_{(2,17), v_t=1}$	6.14e-05	82	241.5
235501.6832	A	$20_{(3,18), v_t=1}$	$19_{(3,17), v_t=1}$	6.14e-05	82	241.5
236998.1508	A	$21_{(1,20), v_t=1}$	$20_{(1,19), v_t=1}$	1.01e-04	86	245.0
236998.1508	A	$21_{(2,20), v_t=1}$	$20_{(2,19), v_t=1}$	1.01e-04	86	245.0
236998.1508	A	$21_{(1,20), v_t=1}$	$20_{(2,19), v_t=1}$	1.42e-07	86	245.0
236998.1508	A	$21_{(2,20), v_t=1}$	$20_{(1,19), v_t=1}$	1.42e-07	86	245.0
244889.6209	A	$20_{(3,17), v_t=1}$	$19_{(3,16), v_t=1}$	2.42e-05	82	249.1
244889.6209	A	$20_{(4,17), v_t=1}$	$19_{(4,16), v_t=1}$	2.42e-05	82	249.1
244889.6209	A	$20_{(3,17), v_t=1}$	$19_{(4,16), v_t=1}$	7.48e-05	82	249.1
244889.6209	A	$20_{(4,17), v_t=1}$	$19_{(3,16), v_t=1}$	7.48e-05	82	249.1
245237.0813	A	$12_{(11,1), v_t=1}$	$11_{(10,2), v_t=1}$	7.14e-05	50	187.2
245444.9402	E	$11_{(11,1), v_t=0}$	$10_{(10,1), v_t=0}$	8.23e-05	46	70.1
246179.2041	A	$21_{(2,19), v_t=1}$	$20_{(3,18), v_t=1}$	3.88e-05	86	253.3
246179.2041	A	$21_{(3,19), v_t=1}$	$20_{(2,18), v_t=1}$	3.88e-05	86	253.3
246179.2041	A	$21_{(2,19), v_t=1}$	$20_{(2,18), v_t=1}$	6.89e-05	86	253.3
246179.2041	A	$21_{(3,19), v_t=1}$	$20_{(3,18), v_t=1}$	6.89e-05	86	253.3
246481.9960	A	$19_{(3,16), v_t=2}$	$18_{(4,15), v_t=2}$	6.01e-05	78	309.9
246584.8477	E	$18_{(5,13), v_t=0}$	$17_{(6,12), v_t=0}$	6.11e-05	74	129.1
246584.8511	E	$18_{(6,13), v_t=0}$	$17_{(6,12), v_t=0}$	2.23e-05	74	129.1
246584.8724	E	$18_{(5,13), v_t=0}$	$17_{(5,12), v_t=0}$	2.23e-05	74	129.1
246584.8759	E	$18_{(6,13), v_t=0}$	$17_{(5,12), v_t=0}$	6.11e-05	74	129.1
250237.9675	E	$23_{(0,23), v_t=1}$	$22_{(0,22), v_t=1}$	1.11e-04	94	251.9
250237.9675	E	$23_{(1,23), v_t=1}$	$22_{(1,22), v_t=1}$	1.11e-04	94	251.9
250237.9675	E	$23_{(0,23), v_t=1}$	$22_{(1,22), v_t=1}$	1.54e-05	94	251.9
250237.9675	E	$23_{(1,23), v_t=1}$	$22_{(0,22), v_t=1}$	1.54e-05	94	251.9

**Table B.3.** Spectroscopic data of the gGg' ethylene glycol lines displayed in Fig. 4

frequency (MHz)	Quantum number <sup>a</sup>		$A_{ul}$ (s <sup>-1</sup> )	$g_{up}$	$E_{up}$ (K)
	$J_{K_a, K_c}, v(\text{up})$	$J_{K_a, K_c}, v(\text{low})$			
217539.718	22 <sub>(2,20),v=0</sub>	21 <sub>(2,19),v=1</sub>	1.495E-04	315	126.6
218712.336	22 <sub>(3,20),v=1</sub>	21 <sub>(3,19),v=0</sub>	1.512E-04	315	126.7
220249.787	22 <sub>(2,20),v=1</sub>	21 <sub>(2,19),v=0</sub>	1.550E-04	405	126.7
229906.833	24 <sub>(2,23),v=1</sub>	23 <sub>(1,22),v=1</sub>	1.013E-04	343	142.7
231212.070	24 <sub>(1,23),v=1</sub>	23 <sub>(1,22),v=0</sub>	1.210E-04	441	142.7
231366.043	25 <sub>(1,25),v=0</sub>	24 <sub>(1,24),v=1</sub>	1.185E-04	357	147.0
231366.176	25 <sub>(0,25),v=0</sub>	24 <sub>(0,24),v=1</sub>	1.184E-04	459	147.0
232706.108	25 <sub>(0,25),v=1</sub>	24 <sub>(1,24),v=1</sub>	1.199E-04	357	147.1
232706.561	25 <sub>(1,25),v=1</sub>	24 <sub>(0,24),v=1</sub>	1.201E-04	459	147.1
233690.540	22 <sub>(4,18),v=1</sub>	21 <sub>(4,17),v=0</sub>	1.118E-04	405	134.2
234047.938	25 <sub>(1,25),v=1</sub>	24 <sub>(1,24),v=0</sub>	1.225E-04	459	147.1
234048.079	25 <sub>(0,25),v=1</sub>	24 <sub>(0,24),v=0</sub>	1.226E-04	357	147.1
234150.007	23 <sub>(8,15),v=0</sub>	22 <sub>(8,14),v=1</sub>	1.039E-04	423	166.1
236771.321	23 <sub>(6,17),v=0</sub>	22 <sub>(6,16),v=1</sub>	1.139E-04	423	153.1
236845.214	23 <sub>(7,17),v=1</sub>	22 <sub>(7,16),v=0</sub>	1.102E-04	423	159.0
236864.590	23 <sub>(3,20),v=1</sub>	22 <sub>(3,19),v=0</sub>	1.058E-04	329	142.4
245205.575	25 <sub>(2,23),v=0</sub>	24 <sub>(3,22),v=0</sub>	1.714E-04	459	160.6
245215.148	24 <sub>(7,18),v=0</sub>	23 <sub>(7,17),v=1</sub>	1.232E-04	441	170.8
245238.282	24 <sub>(12,12),v=1</sub>	23 <sub>(12,11),v=0</sub>	1.016E-04	441	216.4
245238.282	24 <sub>(12,13),v=1</sub>	23 <sub>(12,12),v=0</sub>	1.016E-04	343	216.4
245424.852	24 <sub>(11,14),v=1</sub>	23 <sub>(11,13),v=0</sub>	1.073E-04	343	205.3
245424.853	24 <sub>(11,13),v=1</sub>	23 <sub>(11,12),v=0</sub>	1.073E-04	441	205.3
245681.514	24 <sub>(10,15),v=1</sub>	23 <sub>(10,14),v=0</sub>	1.126E-04	343	195.2
245681.559	24 <sub>(10,14),v=1</sub>	23 <sub>(10,13),v=0</sub>	1.126E-04	441	195.2
245742.900	24 <sub>(6,19),v=0</sub>	23 <sub>(6,18),v=1</sub>	1.280E-04	441	164.8
246042.955	24 <sub>(9,16),v=1</sub>	23 <sub>(9,15),v=0</sub>	1.176E-04	343	186.0
246044.081	24 <sub>(9,15),v=1</sub>	23 <sub>(9,14),v=0</sub>	1.176E-04	441	186.0
250230.085	19 <sub>(4,15),v=0</sub>	18 <sub>(3,15),v=1</sub>	1.043E-04	351	102.1
250473.822	25 <sub>(4,22),v=0</sub>	24 <sub>(4,21),v=1</sub>	1.059E-04	357	166.5

**Notes.**

<sup>(a)</sup> Tunnelling is observed between two equivalent equilibrium configurations and splits each rotational level into two distinct states designated  $v = 0$  and  $v = 1$  (BD15).



## Appendix C: Contamination

Figure C.1 shows that the acetic acid emission at 219016 MHz is partially contaminated by the emission from an unidentified species towards the northwest region from the EGP peak.

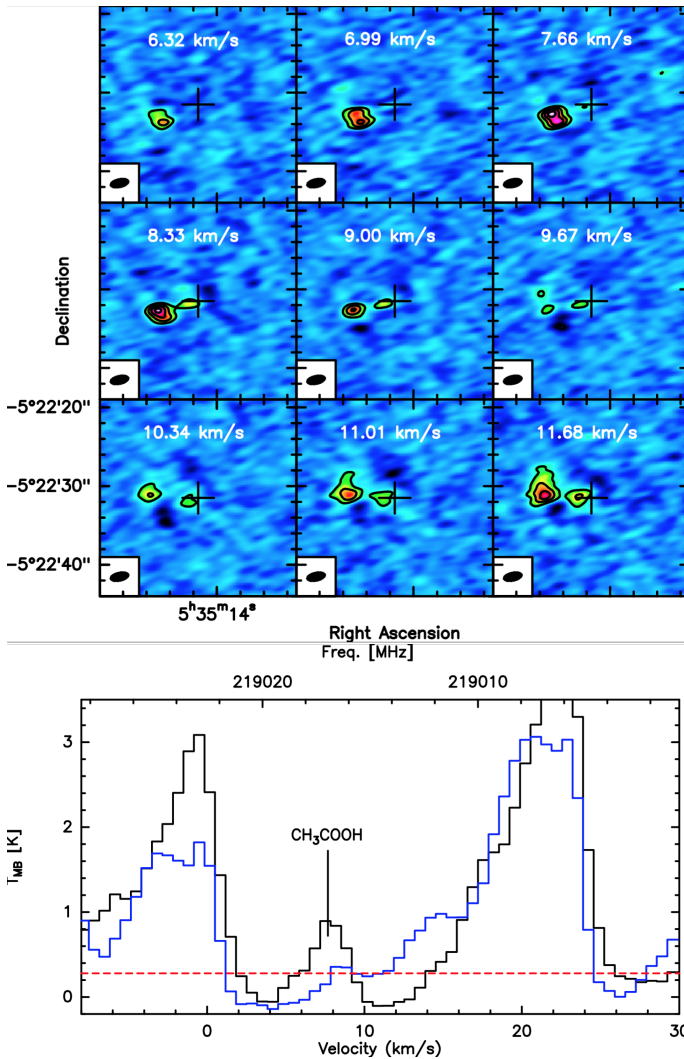


**Fig. C.1.** *Top Panel:*  $\text{CH}_3\text{COOH}$  channel emission maps at 219016 MHz. *Bottom Panel:* Spectra centred at 219016 MHz. The black spectrum is taken in direction of the EGP emission peak while the blue one is taken in direction of the northwest clump which contaminates the  $\text{CH}_3\text{COOH}$  emission maps displayed here as well as in Figure 1. The red dashed line shows the  $3\sigma$  noise level of the spectrum taken in direction of the northwest clump.

## Appendix D: Comparison with the $\text{HCOOCH}_3$ emission

Figure D.1 illustrates the fact the distribution of the emission associated with the acetic acid and the ethylene glycol molecules differs from that of typical O-bearing species, such as methyl formate ( $\text{HCOOCH}_3$ ) within Orion-KL.

## Appendix E: $\text{HC}_3\text{N}$ molecular ring and acetic acid and ethylene glycol emission

The three panels of Figure E.1 show the  $\text{HC}_3\text{N}$  ring-like structure emission (Wright & Plambeck 2017) overlaid with the emission

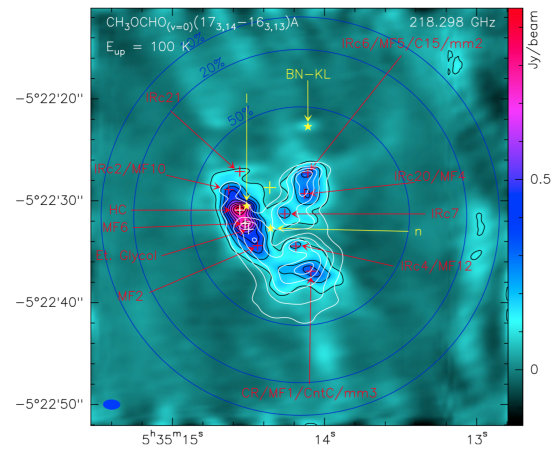


**Fig. D.1.** Continuum emission at 1.3mm (color) overlaid with the  $\text{HCOOCH}_3$  (white contours) emission at 218298 MHz. Positions of the sources analysed in our Paper I are also given.

of acetic acid, aGg'-ethylene glycol and gGg'-ethylene glycol towards the Orion Kleinmann-Low nebula.

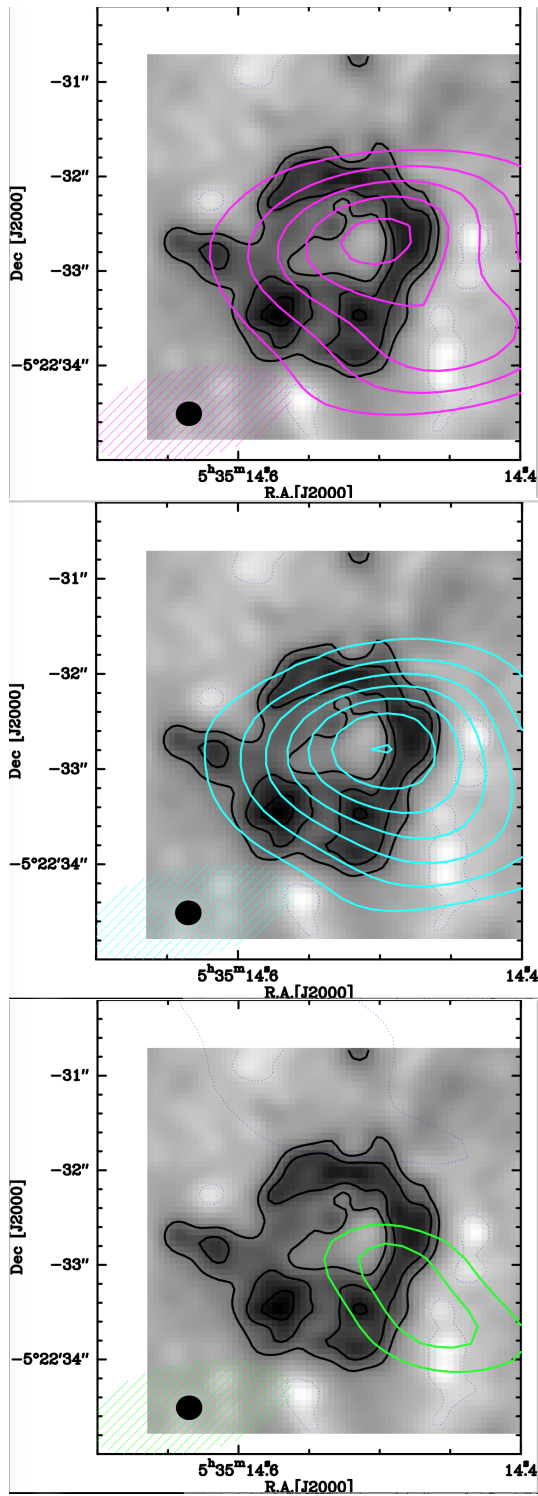


**Fig. E.1.** ALMA observations of the  $\text{HC}_3\text{N}$  emission at 354.69 GHz (in grey scale, see Wright & Plambeck 2017) overlaid with the emission of acetic acid (purple contours, top panel), aGg'-ethylene glycol (cyan contours, middle panel) and gGg'-ethylene glycol (green contours, bottom panel). The ALMA synthesized beams are shown as the black circles for the  $\text{HC}_3\text{N}$  data (Wright & Plambeck 2017) and as colored ellipses for our data.

**Table B.2.** Spectroscopic data of the aGg' ethylene glycol lines displayed in Fig. 3

Frequency (MHz)	Quantum number <sup>a</sup>		$A_{u,l}$ $s^{-1}$	$g_{up}$	$E_{up}$ (K)
	$J_{K_a,K_c},v(up)$	$J_{K_a,K_c},v(low)$			
216614.952	20 <sub>(3,17),v=1</sub>	19 <sub>(3,16),v=0</sub>	2.222E-04	369	110.8
216685.815	21 <sub>(3,19),v=1</sub>	20 <sub>(3,18),v=0</sub>	2.030E-04	387	117.3
216826.112	20 <sub>(5,15),v=1</sub>	19 <sub>(5,14),v=0</sub>	1.792E-04	369	116.8
217139.723	21 <sub>(4,17),v=0</sub>	20 <sub>(4,16),v=1</sub>	2.423E-04	387	123.9
217449.995	24 <sub>(1,24),v=0</sub>	23 <sub>(1,23),v=1</sub>	2.520E-04	441	136.4
217450.270	24 <sub>(0,24),v=0</sub>	23 <sub>(0,23),v=1</sub>	2.520E-04	343	136.4
217587.548	21 <sub>(2,19),v=1</sub>	20 <sub>(2,18),v=0</sub>	2.654E-04	301	117.2
218238.988	22 <sub>(17,5),v=0</sub>	21 <sub>(17,4),v=1</sub>	1.018E-04	315	266.2
218238.988	22 <sub>(17,6),v=0</sub>	21 <sub>(17,5),v=1</sub>	1.018E-04	405	266.2
218304.671	22 <sub>(16,6),v=0</sub>	21 <sub>(16,5),v=1</sub>	1.192E-04	315	250.0
218304.671	22 <sub>(16,7),v=0</sub>	21 <sub>(16,6),v=1</sub>	1.192E-04	405	250.0
218371.495	22 <sub>(4,19),v=0</sub>	21 <sub>(4,18),v=1</sub>	1.881E-04	405	132.6
218379.983	22 <sub>(15,7),v=0</sub>	21 <sub>(15,6),v=1</sub>	1.355E-04	315	234.8
218379.983	22 <sub>(15,8),v=0</sub>	21 <sub>(15,7),v=1</sub>	1.355E-04	405	234.8
218705.810	22 <sub>(12,10),v=0</sub>	21 <sub>(12,9),v=1</sub>	1.786E-04	315	195.1
218705.810	22 <sub>(12,11),v=0</sub>	21 <sub>(12,10),v=1</sub>	1.786E-04	405	195.1
218872.112	22 <sub>(11,12),v=0</sub>	21 <sub>(11,11),v=1</sub>	1.911E-04	405	183.8
218872.112	22 <sub>(11,11),v=0</sub>	21 <sub>(11,10),v=1</sub>	1.911E-04	315	183.8
219089.720	22 <sub>(10,13),v=0</sub>	21 <sub>(10,12),v=1</sub>	2.027E-04	405	173.5
219089.728	22 <sub>(10,12),v=0</sub>	21 <sub>(10,11),v=1</sub>	2.027E-04	315	173.5
219385.178	22 <sub>(9,14),v=0</sub>	21 <sub>(9,13),v=1</sub>	2.136E-04	405	164.3
219385.426	22 <sub>(9,13),v=0</sub>	21 <sub>(9,12),v=1</sub>	2.136E-04	315	164.3
219540.443	22 <sub>(2,21),v=1</sub>	21 <sub>(2,20),v=0</sub>	2.539E-04	315	122.1
219580.672	22 <sub>(1,21),v=1</sub>	21 <sub>(1,20),v=0</sub>	2.568E-04	405	122.0
219764.926	20 <sub>(4,16),v=1</sub>	19 <sub>(4,15),v=0</sub>	2.454E-04	369	113.5
219809.406	22 <sub>(8,14),v=0</sub>	21 <sub>(8,13),v=1</sub>	2.238E-04	315	156.0
220496.592	22 <sub>(7,15),v=0</sub>	21 <sub>(7,14),v=1</sub>	2.339E-04	315	148.8
229816.573	23 <sub>(9,15),v=0</sub>	22 <sub>(9,14),v=1</sub>	2.499E-04	329	175.6
229817.111	23 <sub>(9,14),v=0</sub>	22 <sub>(9,13),v=1</sub>	2.499E-04	423	175.6
230305.630	23 <sub>(8,15),v=0</sub>	22 <sub>(8,14),v=1</sub>	2.610E-04	423	167.4
230472.528	21 <sub>(4,17),v=1</sub>	20 <sub>(4,16),v=0</sub>	2.836E-04	301	124.2
230830.319	24 <sub>(2,22),v=0</sub>	23 <sub>(2,21),v=1</sub>	2.822E-04	343	149.8
230933.676	23 <sub>(3,20),v=0</sub>	22 <sub>(3,19),v=1</sub>	3.166E-04	423	143.3
230965.547	23 <sub>(7,17),v=0</sub>	22 <sub>(7,16),v=1</sub>	2.715E-04	329	160.2
231127.401	23 <sub>(7,16),v=0</sub>	22 <sub>(7,15),v=1</sub>	2.722E-04	423	160.2
231524.033	23 <sub>(6,18),v=0</sub>	22 <sub>(6,17),v=1</sub>	2.714E-04	329	154.1
231564.005	24 <sub>(1,24),v=1</sub>	23 <sub>(1,23),v=0</sub>	3.043E-04	343	136.8
231564.320	24 <sub>(0,24),v=1</sub>	23 <sub>(0,23),v=0</sub>	3.043E-04	441	136.8
232350.059	22 <sub>(10,13),v=1</sub>	21 <sub>(10,12),v=0</sub>	2.420E-04	315	173.8
232350.068	22 <sub>(10,12),v=1</sub>	21 <sub>(10,11),v=0</sub>	2.420E-04	405	173.8
232597.215	22 <sub>(9,14),v=1</sub>	21 <sub>(9,13),v=0</sub>	2.549E-04	315	164.6
232597.490	22 <sub>(9,13),v=1</sub>	21 <sub>(9,12),v=0</sub>	2.548E-04	405	164.6
232881.533	23 <sub>(6,17),v=0</sub>	22 <sub>(6,16),v=1</sub>	2.607E-04	423	154.3
232987.353	22 <sub>(8,14),v=1</sub>	21 <sub>(8,13),v=0</sub>	2.669E-04	405	156.3
233536.696	22 <sub>(5,18),v=1</sub>	21 <sub>(5,17),v=0</sub>	2.930E-04	315	137.7
233561.785	22 <sub>(7,16),v=1</sub>	21 <sub>(7,15),v=0</sub>	2.785E-04	315	149.1
233664.319	22 <sub>(7,15),v=1</sub>	21 <sub>(7,14),v=0</sub>	2.788E-04	405	149.1
234264.446	22 <sub>(6,17),v=1</sub>	21 <sub>(6,16),v=0</sub>	2.839E-04	315	143.0
235304.050	22 <sub>(6,16),v=1</sub>	21 <sub>(6,15),v=0</sub>	2.897E-04	405	143.1
235600.179	23 <sub>(2,21),v=1</sub>	22 <sub>(2,20),v=0</sub>	3.276E-04	329	138.7
235620.372	24 <sub>(4,21),v=0</sub>	23 <sub>(4,20),v=1</sub>	2.881E-04	441	155.4
235834.240	26 <sub>(1,26),v=0</sub>	25 <sub>(1,25),v=1</sub>	3.222E-04	477	159.3
235834.327	26 <sub>(0,26),v=0</sub>	25 <sub>(0,25),v=1</sub>	3.221E-04	371	159.3
244879.919	23 <sub>(6,18),v=1</sub>	22 <sub>(6,17),v=0</sub>	3.028E-04	423	154.4
245022.738	27 <sub>(1,27),v=0</sub>	26 <sub>(1,26),v=1</sub>	3.616E-04	385	171.4
245022.787	27 <sub>(0,27),v=0</sub>	26 <sub>(0,26),v=1</sub>	3.617E-04	495	171.4
246387.881	23 <sub>(6,17),v=1</sub>	22 <sub>(6,16),v=0</sub>	3.280E-04	329	154.6
250300.410	25 <sub>(10,16),v=0</sub>	24 <sub>(10,15),v=1</sub>	3.208E-04	357	209.0
250300.508	25 <sub>(10,15),v=0</sub>	24 <sub>(10,14),v=1</sub>	3.209E-04	459	209.0

**Table B.2.** Continued.

Frequency (MHz)	Quantum number <sup>a</sup>		$A_{u,l}$ (s <sup>-1</sup> )	$g_{up}$	$E_{up}$ (K)
	$J_{K_a,K_c},v(\text{up})$	$J_{K_a,K_c},v(\text{low})$			
250487.421	23 <sub>(5,18),v=1</sub>	22 <sub>(5,17),v=0</sub>	3.606E-04	329	150.3
250731.885	25 <sub>(9,17),v=0</sub>	24 <sub>(9,16),v=1</sub>	3.341E-04	357	199.8
250734.147	25 <sub>(9,16),v=0</sub>	24 <sub>(9,15),v=1</sub>	3.341E-04	459	199.8
251382.563	25 <sub>(8,17),v=0</sub>	24 <sub>(8,16),v=1</sub>	3.471E-04	459	191.6
251473.045	25 <sub>(6,20),v=0</sub>	24 <sub>(6,19),v=1</sub>	1.607E-04	357	178.4
251574.351	27 <sub>(2,26),v=0</sub>	26 <sub>(2,25),v=1</sub>	3.873E-04	385	179.3
251577.144	27 <sub>(1,26),v=0</sub>	26 <sub>(1,25),v=1</sub>	3.870E-04	495	179.3

**Notes.**

<sup>(a)</sup> Tunnelling is observed between two equivalent equilibrium configurations and splits each rotational level into two distinct states designated as  $v = 0$  and  $v = 1$  (BD15).